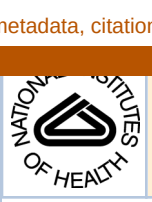

Published in final edited form as:
J Struct Biol. 2013 September ; 183(3): . doi:10.1016/j.jsb.2013.06.011.

Stress-vs-time signals allow the prediction of structurally catastrophic events during fracturing of immature cartilage and predetermine the biomechanical, biochemical, and structural impairment

Bernd Rolauffs[1,2,*], **Bodo Kurz**[3,4], **Tino Felka**[1], **Miriam Rothdiener**[1], **Tatiana Uynuk-Ool**[1], **Matthias Aurich**[5], **Eliot Frank**[2], **Christian Bahrs**[1], **Andreas Badke**[1], **Ulrich Stöckle**[1], **Wilhelm K. Aicher**[6], and **Alan J. Grodzinsky**[2]

[1]Siegfried Weller Institute for Trauma Research, BG Trauma Clinic, Eberhard Karls University, 72076 Tuebingen, Germany

[2]Massachusetts Institute of Technology, Center for Biomedical Engineering, Cambridge, MA 02319, USA

[3]Faculty of Health Sciences and Medicine, Bond University, Gold Coast, Queensland 4226 Australia

[4]Anatomical Institute, Christian-Albrechts-University, 24098 Kiel, Germany

[5]Department of Orthopaedic and Trauma Surgery, Elblandklinikum Riesa, 01589 Riesa, Germany

[6]Department of Urology, Eberhard Karls University, 72072 Tuebingen, Germany.

Abstract

Objective—Trauma-associated cartilage fractures occur in children and adolescents with clinically significant incidence. Several studies investigated biomechanical injury by compressive forces but the injury-related stress has not been investigated extensively. In this study, we hypothesized that the biomechanical stress occurring during compressive injury predetermines the biomechanical, biochemical, and structural consequences. We specifically investigated whether the stress-vs-time signal correlated with the injurious damage and may allow prediction of cartilage matrix fracturing.

Methods—Superficial and deeper zones disks (SZDs, DZDs; immature bovine cartilage) were biomechanically characterized, injured (50% compression, 100%/sec strain-rate), and re-characterized. Correlations of the quantified functional, biochemical and histological damage with biomechanical parameters were zonally investigated.

Results—Injured SZDs exhibited decreased dynamic stiffness (by 93.04 ± 1.72%), unresolvable equilibrium moduli, structural damage (2.0 ± 0.5 on a 5-point-damage-scale), and 1.78-fold increased sGAG loss. DZDs remained intact. Measured stress-vs-time-curves during injury displayed 4 distinct shapes, which correlated with histological damage ($p<0.001$), loss of dynamic

[*]To whom correspondence should be addressed: Siegfried Weller Institute for Trauma Research, BG Trauma Clinic, Schnarrenbergstr 95, 72076 Tuebingen, Germany; Phone: +49-7071-6060; berndrolauffs@googlemail.com.

stiffness and sGAG ($p<0.05$). Damage prediction in a blinded experiment using stress-vs-time grades was 100%-correct and sensitive to differentiate single/complex matrix disruptions. Correlations of the dissipated energy and maximum stress rise with the extent of biomechanical and biochemical damage reached significance when SZDs and DZDs were analyzed as zonal composites but not separately.

Conclusion—The biomechanical stress that occurs during compressive injury predetermines the biomechanical, biochemical, and structural consequences and, thus, the structural and functional damage during cartilage fracturing. A novel biomechanical method based on the interpretation of compressive yielding allows the accurate prediction of the extent of structural damage.

Introduction

Articular cartilage lesions of the adult knee joint are common[1]. In children and adolescents, the incidence of articular cartilage lesions varies depending on the cause and time of clinical presentation and the patient age. However, cartilage lesions in children and adolescents always occur with clinically significant incidence[2-10] and are, in some studies, considered the most common type of defect after trauma[2, 10]. Three studies reported the use of autologous chondrocyte implantation in the adolescent population[11-13] illustrating the increasing awareness of the surgical community on the clinical significance of cartilage lesions in the skeletally immature knee joint.

Macroscopically, four types of traumatic cartilage lesions are classified[14]. Their morphology is associated with different mechanisms of trauma such as shear or blunt impact[14]. For example, impact trauma leads to a stellate fracture of the cartilage[14] and, on tissue levels, to fissuring[15, 16], cell death[15, 17], and impaired collagen integrity[16, 18, 19]. In both immature and mature cartilages, traumatic lesions begin with damage to the articular surface as clinical and basic science studies demonstrated[14-19]. That the damage is localized to the articular surface can be explained by the presence of depth-dependent variations in the structural[16, 20], biochemical[16, 21] and biomechanical[16, 22] properties.

Several previous studies investigated the biomechanical properties of articular cartilage[23-28] and the consequences of injury by compressive forces[16, 29-34]. However, to the best of our knowledge, the biomechanical stress (force per area) that occurs *during* injurious compression has not been investigated extensively[16, 31]. For example, studies examined the peak stress and the strain rate as parameters defining injury[33, 35, 36] but few attempts have been made to specifically investigate the biomechanical environment *during* an impact injurious compression[37]. Consequently, our knowledge of the stress-vs-time profile that occurs during injurious compression and specifically the interconnections of the stress with the extent of damage are still limited. Such insight, however, is relevant for understanding the initial events during injury and, ultimately, for the development of articular cartilage lesions and posttraumatic osteoarthritis.

In this study, we investigated the biomechanical stress that occurs during injurious compression. Because impact trauma causes a specific stellate cartilage fracture[14], we hypothesized that the rise and time-course of stress during compressive injury largely determine the extent of the damage. Thus, we investigated whether the stress-vs-time signal that was recorded during injurious compression correlated with the biochemical, biomechanical and structural cartilage damage. Secondly, we investigated whether it was possible to accurately predict the extent of damage by utilizing the stress-vs-time signal in a blinded experimental approach. Finally, because damage to immature cartilage does not progress beyond the superficial zone[16], we asked whether cartilage compressive properties exhibit a step-wise change with depth into the tissue similar to the depth-dependent change

in shear properties below the superficial zone reported previously[23, 24]. Since cartilage can generally be considered a composite of materials having differing properties[38, 39], we tested the concept that immature articular cartilage, in particular, functions as a bilayer composite of superficial and deeper zone materials. We chose immature cartilage for this study due to the emerging clinical relevance of cartilage lesions in children and adolescents[2-10].

Methods

Superficial and Deeper Zone Articular Cartilage Disks

Full-thickness cylindrical bovine articular cartilage explants (3mm diameter, n=32) including the intact superficial zone were harvested from the weight-bearing areas of the condyles and patellofemoral grooves of 1-2 week old calves (n=3) within 24h of death. Explants were equilibrated in 5% CO_2 in DMEM with 10% FBS, 10nM HEPES, 1nM sodium pyruvate, 0.1mM non-essential amino acids, 0.4mM proline, 20μg/ml ascorbic acid plus antibiotics[36]. Explants were sliced perpendicular to the longitudinal axis into 200–400μm-thick superficial zone disks including the articular surface (SZDs; n=32) and deeper zone disks (DZDs; ~1300μm; n=32; see Fig. 1A schematic).

Cartilage Thickness and Biomechanical Properties

Each disk (n=64) was placed within the well of a loading chamber with an upper platen attached to an incubator-housed loading instrument[40]. Thickness was measured individually for each disk by applying a slow compression ramp (20μm/sec ramp speed) with automated compression interrupt caused by an increase in offset load indicating contact between platen and disk. Utilizing the measured thickness of each SZD and corresponding DZD, we calculated the “depth position” of the center of each disk with respect to the articular surface (see Fig. 1A schematic).

To determine the mechanical properties of each SZD and DZD, three successive displacement-controlled ramp-and-hold compressions to final strains of 10% (200-sec compression, 600-sec hold), 12.5% and 15% (30-sec compression, 300-sec hold) were applied in unconfined compression. The resulting equilibrium loads (after stress relaxation) were used to compute the unconfined equilibrium moduli. At 15% final offset strain, each disk was then subjected to 3% dynamic strain amplitude at 1.0 and 0.1Hz to compute the dynamic stiffnesses at each frequency[36].

Biomechanical Injury

After biomechanical characterization, each disk was equilibrated (20min) and then subjected to injurious compression (unconfined) to a final strain of 50% at 100%/sec strain rate (“injury”). During injury, the stress was continuously measured by the loading instrument[40]. After 5min of unconfined re-swelling, the disks were biomechanically re-characterized. Note in this context that some injured samples were macroscopically and microscopically damaged. As consequence, the geometrical shape of these samples was altered, and the re-characterization was to assess the effective macroscopic unconfined compression properties of the resulting injured explants.

Biochemical Properties

After injury, SZDs (n=19) and DZDs (n=20) were incubated (48h, 37°C, 5%CO_2), then solubilized overnight at 60°C in 500μg/ml proteinase-K. sGAG content and sGAG loss to the medium were assessed using the dimethylmethylene-blue-dye-binding-assay with shark chondroitin sulfate as the standard[41]. sGAG loss to the medium was determined after 48h incubation. The medium was snap-frozen, lyophilized, resuspended and analyzed. Control

disks for biochemical analyses were biomechanically tested, re-tested after 25 min equilibration, but not injured.

Stress-vs-Time Analyses

The load-vs-time signals were recorded during compression injury of each disk. From the recorded load, the stress was calculated. The stress-vs-time signals were used to compute best-fit rational functions and their first derivatives (TableCurve-2D-5.01, Systat, Chicago) using the resulting R^2 of the fitting procedure as a parameter of goodness-of-fit. This enabled quantification of the critical and inflection points and consequently the grading of the stress-vs-time signals using a 4-point-scale (detailed description: Fig. 2 legend). We then investigated correlations of the stress-vs-time-grades with specific parameters that describe biomechanical and biochemical impairment after injury. For each stress-vs-time curve, we calculated the running derivative of stress-vs-time, i.e. the rate of change of the stress-vs-time signal. Based on these values, we determined the maximum stress rise during injury (for example, in Fig 2A the maximum stress rise is located where the maximum absolute value of the first derivative is localized: at time=0.48sec). In addition, the integral of each stress-vs-strain curve was calculated to obtain the energy that was dissipated within each cartilage disk during injury (n=64).

Articular Cartilage Damage Score

To quantify tissue damage, SZDs (n=13) and DZDs (n=12) were injured and, along with corresponding control disks, snap-frozen in liquid nitrogen, fixed in 10% paraformaldehyde and paraffin-embedded. 6μm sections were stained with Safranin-O/fast green, photographed and graded by a blinded investigator using a 5-point-scale as described[16] (detailed description: Fig. 6 legend).

Histological Damage Prediction after Severe Biomechanical Injury

Because our data demonstrated that the stress-vs-time-grades correlated with the presence of histological damage (see Results), we performed additional experiments asking whether this correlation may be suitable for the *prediction* of histological damage. 10 intact disks (consisting of both superficial and deeper zones) were subjected to injurious compression using 65% strain at 100%/sec strain-rate to increase the amount of structural damage ("*severe* injury"). The recorded stress-vs-time signals were graded (BR) on a 4-point-scale (see Fig. 2 legend). Grade 3 disks were predicted to be structurally damaged. A second observer (BK, blinded to the grading) performed serial horizontal sectioning, Alcian-blue staining, and assessed the number of serial sections containing structural disruptions. The predicted damage extent was compared with the histological results.

Statistical Analysis

All data are presented as mean ± SEM. Data were analyzed for normality (Kolmogorov-Smirnov-test). Normally distributed data were subjected to the Student's *t*-test for matched pairs; non-normal data were subjected to the Mann-Whitney-Rank-Sum-Test. Differences were considered significant at $p<0.05$. A generalized linear mixed effects model with animal as a random variable was used for further analyses; our calculations demonstrated that the random variable animal had no significant effect. Using Pearson-Product-Moment-Correlation-tests, the level of significance was calculated for the correlations tested. Linear and non-linear regression (exponential, logarithmic, polynomial, power) were performed on data from SZDs alone, DZDs alone, and on statistically combined data sets from both SZDs and DZDs (that, however, were biomechanically tested separately). This procedure enabled assessment of whether (and how) specific parameters examined correlated with tissue depth within either the SZ or DZ, or whether a depth-dependency was only present when

statistically combined data sets of both zones were investigated (Table I: S, D, and S&D; example: Figure 1B). Calculations were performed with Microsoft-Excel 2010 and SigmaPlot-11.0.0.77 (Systat, Chicago).

Results

Biomechanical Properties

The equilibrium modulus and the dynamic stiffness of normal, uninjured SZDs (0.24 ± 0.06MPa; 1.71 ± 0.39MPa at f=1Hz) were significantly lower than those of the DZDs (0.66 ± 0.05MPa; 12.09 ± 0.64MPa at f=1Hz; $p<0.001$; Fig. 1B). The magnitudes of the moduli were comparable to those of our previous study[16], as were the ratios deeper-to-superficial zone moduli (equilibrium modulus ratio: 2.62; dynamic stiffness ratio: 7.32).

Injury

During injurious compression, peak stresses were 15.33-fold lower in SZDs (0.88 ± 0.21MPa) than DZDs (13.49 ± 0.69MPA; $p<0.0001$, Fig. 3A). The absolute values of the maximum stress rise were significantly lower during the compression phase of injury than during release ($p<0.001$) and significantly lower for SZDs than DZDs ($p<0.001$; compression/superficial: 8.29 ± 1.37MPa/sec; compression/deep: 48.05 ± 1.58MPa/sec; release/superficial: 10.89 ± 1.77MPa/sec; release/deep: 60.77 ± 2.09MPa/sec; Fig. 3B). Thus, DZDs exhibited a maximum stress rise for both compression and release that were 12.69- and 8.03-fold higher than for SZDs ($p<0.001$). During injury, energy dissipation was 20-fold higher in DZDs than SZDs (superficial: 0.48 ± 0.08Jx$10^3/\mu m^3$; deep: 9.60 ± 1.15 Jx$10^3/\mu m^3$; $p<0.001$).

Histological Damage

After injurious compression, we observed in 4 of 32 injured SZDs (Fig. 6A-C) macroscopically visible damage and tissue compaction (SZDs: compaction by 20.31 ± 4.31%, DZDs: 7.8 ± 0.47% of their original thickness; $p<0.001$). Microscopically visible tissue damage occurred in SZDs (damage score of 2.0 ± 0.5 on a 5-point-scale; Fig. 6D). As consequence, the geometrical shape of these damaged SZD was altered, and hereafter we will refer to all SZDs as SZDE (superficial zone damaged explant). DZDs and non-injured control disks remained undamaged (damage score: 0; $p<0.001$). All macroscopically damaged SZDEs had grade 3 stress-vs-time signals (double tip in the stress-vs-time signal; i.e. Fig. 2D).

Biomechanical Impairment

After injury, SZDEs suffered extensive functional damage. The dynamic stiffness of SZDEs was significantly decreased by 93.04 ± 1.72% of the pre-injury values ($p<0.0001$; f=1Hz; Fig. 4). The effective equilibrium moduli of the SZDEs were so low that they were not resolvable, indicating functional destruction as we have demonstrated previously[16]. In contrast, DZDs showed less functional damage. The dynamic stiffness of DZDs was significantly decreased by 28.11 ± 1.99% ($p<0.0001$; f=1Hz; Fig. 4) though the equilibrium moduli decreased by only 6.16 ± 1.88% ($p<0.0001$). After injury, the ratio of the DZDs-to-SZDEs dynamic stiffness was increased to 44.59; the pre-injury ratio of these disks was 5.12.

Biochemical Impairment

48h after injury, SZDEs showed a significant 1.78-fold increase in sGAG loss into the medium compared to non-injured SZDEs ($p<0.004$), which released only 10.01 ± 0.55%

sGAG over the same time period. In contrast, injured DZDs showed a significant 0.78-fold decrease ($p<0.05$) in sGAG loss compared to non-injured DZDs (Fig. 5).

Stress-vs-Time Analyses

The recorded stress-vs-time signals were used to compute best-fit rational functions and their first derivatives (TableCurve-2D-5.01, Systat, Chicago). 57% were curve-fit to standard-rationals, 37% to log(x)-rationals, and 6% to Chebyshev-rationals. The resulting R^2 of the fitting procedure as a parameter of goodness-of-fit was $R^2=0.997 \pm 0.0004$.

The stress-vs-time signals exhibited 4 distinctly different shapes (Fig. 2A-D), for which the following grading scale was introduced: Grade 0 resembled the letter "V" with both the descending and ascending parts symmetrical and was considered the ideal stress response. Its derivative was characterized by 1 critical and 2 inflection points. Grade 1 displayed a slight irregularity within the time-derivative (stress rise). The derivative revealed a lower magnitude stress rise over time, though still characterized by 1 critical and 2 inflection points. Grade 2 displayed a derivative that showed a local decrease with time during the compression phase. This derivative was characterized by 1 critical point and 4 inflection points. Grade 3 displayed a regular stress rise but the presence of a double tip instead of a single tip at the transition from compression to relaxation. This occurrence indicated a pronounced stress loss during the final stage of injurious compression during which a stress rise but not a stress loss would be expected. The derivative was characterized by 3 critical points and 4 inflection points. The stress-vs-time signals were graded as follows: SZDEs: grade 0: n=10 (15%), grade 1: n=11 (18%), grade 2: n=7 (10%), grade 3: n=4 (6%); DZDs: grade 0: n=7 (10%); grade 1: n=15 (25%); grade 2: n=10 (16%); grade 3: n=0 (0%). Only 4 SZDEs were grade 3 (6.25% of all disks; 12.5% of all SZDEs); there were no grade 3 DZDs. For correlations of the stress-vs-time signal grades with the presence of histological damage see Fig. 2E-H, Fig. 6, and the result section "Histological Damage".

Histological Damage Prediction

After *severe* injury, 6 of 10 disks showed grade 3 and a seventh showed grade 2 stress-vs-time signals. Each of these disks exhibited extensive structural disruption that was clearly visible in 75.31 ± 5.14% of all serial sections (Fig. 7BC). In 5 of these cases, the stress-vs-time signal contained a double tip. Histologically, a single matrix disruption was present (Fig. 7B). In 2 cases, the stress-vs-time signal contained a triple tip. These disks showed structural disruptions that pervaded the disk horizontally in a y-shape with a common trunk and two extensions roughly perpendicular to each other (Fig. 7C). The remaining 3 of 10 *severely* injured disks had grade 1 stress-vs-time curves. Those disks had some but significantly less damage ($p<0.05$; 55.66 ± 3.54% of all serial sections).

Effects of Disk Thickness and Zonal Origin on Peak Stress and Stress-vs-Time Grades

To assess the effect of disk thickness and zonal origin on the resulting peak stress during injury and on the stress-vs-time grades, 3 additional sets of disks with retained superficial zone (rSZ; n=28) were prepared with thicknesses ranging from 250-420μm, 420-600μm, and 600-1000μm. These 3 sets of rSZ disks were compared to 3 sets of DZDs prepared with comparable thickness ranges (Fig. 8A). When comparing the rSZ disks and the DZDs, the peak stress was significantly different for all 3 sets of thicknesses ($p<0.01$) indicating a zonal effect on peak stress during injury. The peak stress was also significantly different when comparing the rSZ disks ranging from 250-420μm and from 420-600μm with the rSZ set ranging from 601-1000μm ($p=0.01$). When comparing the 3 sets of DZDs with different ranges of thickness, the peak stress was also significantly different ($p<0.001$) indicating an effect of thickness on peak stress for both rSZ and DZDs.

The stress-vs-time grades of the pooled rSZ were not significantly different from those of the pooled DZDs. The stress-vs-time grades of the 3 sets of DZDs were not significantly different from each other. Also, the 3 sets of rSZ were not significantly different from each other. These data suggest that there was no significant effect of disk thickness on the stress-vs-time grades. When comparing the stress-vs-time grades across the zones there were no significant differences between rSZ and DZD sets. Overall, there was no effect of disk thickness or zonal origin on the stress-vs-time grades (Fig. 8B).

Displacement-Rate Analyses

The applied nominal injurious strain rate for all disks was 100%/sec. This corresponded to a measured value of the displacement rate for SZDEs of 322.68 ± 26.56μm/sec and for DZDs 1,140.89 ± 55.52μm/sec. In SZDEs, displacement rates were 387.60 ± 50.92μm/sec (stress-vs-time grade 0); 343.91 ± 45.82μm/sec (grade 1); 166.85 ± 23.88μm/sec (grade 2); 313.91 ± 82.90μm/sec (grade 3); DZDs: 1028.15 ± 104.39μm/sec (grade 0); 991.47 ± 66.84μm/sec (grade 1); 1500.67 ± 67.55μm/sec (grade 2). For SZDEs with grade 3 stress-vs-time signals (presence of macroscopic; see below) the displacement rate was 313.91 ± 67.69μm/sec, which was in the midrange of all occurring SZDE displacement rates (max: 632.62μm/sec; min: 82.90μm/sec). Thus, relatively high displacement-rates were not responsible for the occurring histological damage.

Zonal Correlation Analyses

For all potential correlations that we investigated, we calculated the levels of significance using SZD and DZD data as one statistically combined data set, and also using SZD and DZD data separately. With this approach, we were able to answer whether any two given parameters did or did not correlate within a specific zone (i.e., SZD) or across the entire tissue depth (SZD & DZD as a combined data set). In the following section, only correlations with regard to stress-vs-time grades and injury-inflicted damage are presented; all other correlations are given in Table I.

Before injury, both the equilibrium modulus (correlation coefficient (cc): 0.551) and the dynamic stiffness (CC: 0.88) correlated significantly with increasing depth position ($p<0.001$; Fig. 1B) when SZDs and DZDs were analyzed as one statistically combined data set ($p<0.001$; Table I: S&D). When analyzing the disks as two zonally separate data sets, there was no significant effect of depth position on equilibrium modulus; that is, within the superficial zone, there was no significant correlation of equilibrium modulus with depth position; similarly within the deeper zone alone. There was a significant effect of depth position on dynamic stiffness for DZDs ($p<0.05$; cc: 0.54) but not SZDs.

After injury, the damage-inflicted loss of dynamic stiffness correlated significantly with the injury-related parameters depth position (cc: −0.90), peak stress (cc: −0.92), maximum stress rise (cc: 0.83; $p<0.001$; Fig. 3A,B) and energy dissipation (cc: 0.87; $p<0.0001$) when analyzed as statistically combined data set (Table I) but not when SZDEs and DZDs were analyzed separately. Similarly, sGAG loss correlated significantly with the depth position (Fig. 4A; cc: −0.72), peak stress (cc: −0.81), maximum stress rise (Fig. 4B; cc: 0.80), and energy dissipation (cc: 0.81) when injured SZDEs and DZDs were analyzed as one statistically combined data set. The stress-vs-time grades correlated significantly with loss of dynamic stiffness (cc: −0.46; $p<0.05$) and loss of sGAG (cc: 0.37; $p<0.05$) for SZDEs and DZDs combined as one data set. For SZDEs alone, the stress-vs-time grades correlated significantly with the loss of dynamic stiffness (cc: −0.61; $p<0.05$) and also with histological damage (cc: 1.0; $p<0.001$). All histologically damaged SZDEs demonstrated grade 3 stress-vs-time signals (double tip in the stress-vs-time signal; Fig. 2D); both the presence of histological damage (cc: 0.82) and the stress-vs-time signal (cc: 0.82) correlated

significantly with the SZDE damage score ($p<0.001$). After severe injury - the damage prediction experiment - the stress-vs-time grade correlated significantly with the percentage of serial sections that contained structural damage (cc: 0.70; $p<0.05$; Fig. 7) and the type of histological damage (single matrix disruption or complex disruption; cc: 0.84; $p<0.01$).

Overall, most correlations reached significance when both SZDs/SZDEs and DZDs were analyzed as one statistically combined data set (Table I). Thus, these correlations suggest that immature cartilage functions as a bilayer composite material of zones with discrete properties; within each of the two zones, however, the material properties do not vary significantly with depth. However, all parameters quantifying the occurring damage correlated with the stress-vs-time grades.

Discussion

In this study, we hypothesized that the biomechanical stress-vs-time profile occurring during compressive injury largely predetermines the biomechanical, biochemical, and structural consequences. We specifically investigated whether the stress-vs-time signal that was calculated from the recorded load during compressive injury correlated with the biochemical, biomechanical, and structural damage. First, we developed a novel method to analyze the stress that was calculated from the load measured continuously during compressive injury. We noted 4 types of stress-vs-time signals whose different shapes were determined by the stress behavior during injury, and we introduced a grading system for these stress-vs-time signals based on the critical and inflection points of the stress-vs-time derivative (Fig. 2). We then correlated these different waveforms with the extent of structural, biomechanical, and biochemical impairment after injury.

Most importantly, the stress-vs-time grades correlated significantly with the extent of histological damage. In 12% of the injured superficial zone damaged explants (SZDEs), extensive compaction and structural damage had occurred. In these explants, the stress-vs-time signal was graded as 3, and only these signals displayed a double tip of the stress during maximum compression (Fig. 2D). This particular stress waveform was predictive of an abrupt discontinuity in the stress rise by comparison to Figure 2A during the final release phase of injurious compression since, at this instant in time, a stress rise but not a stress discontinuity would be expected in structurally intact cartilage. The stress loss that had occurred was based on stress yielding, a catastrophic structural event visible as extensive histological damage.

Because the stress-vs-time grades correlated with the extent of SZDE structural damage, we investigated the predictability of structural damage based on the stress-vs-time signal. We applied a further "*severe*" injury consisting of a final compressive strain of 65% (strain rate: 100%/sec). One observer graded the stress-vs-time signals whereas a second blinded observer predicted the structural damage by serial horizontal sectioning; the predicted damage extent was compared with the histological results. Of 10 disks, 6 disks were graded as 3 and 1 as grade 2; these 7 were predicted to have suffered extensive structural damage. Indeed, in a top-down view, the disruption in these disks was comparable to arthroscopically stellate-appearing cartilage fractures associated with impact trauma[14]. Interestingly, the disks whose stress signals contained a double tip had suffered a single matrix disruption (Fig. 7B); disks with signals containing a triple tip demonstrated a complex structural disruption pervading the disk in a y-shape (Fig. 7C). Thus, we present a novel biomechanical method based on the interpretation of compressive yielding that allows for the accurate prediction of structural damage caused by injury. Surprisingly, our method was sensitive enough to predict whether catastrophic structural yielding occurred either as a single matrix disruption or a consecutive stepwise sequence of fracture events. Although we

investigated structural yielding of articular cartilage in the context of initial traumatic events ultimately leading to osteoarthritis, the method could be applied in principle to the yielding of other weight-bearing tissues or even non-biological materials.

Next, we demonstrated that the stress-vs-time grades correlated with the loss of dynamic stiffness and the loss of sGAG (when SZDEs and DZDs were analyzed as a combined data set). The stress-vs-time grades also correlated with the loss of dynamic explant properties in SZDEs alone. The loss of dynamic stiffness and sGAG both correlated with depth position, peak stress, energy dissipation, maximum stress rise, and strain rate when SZDEs and DZDs were analyzed as statistically combined data set (Table I). Overall, these correlations highlight how closely the biomechanical stress during compressive injury predetermines its biomechanical, biochemical, and structural consequences.

We also investigated whether the biomechanical properties of immature cartilage exhibited a step-wise increase with depth into the tissue similar to the reported sudden change in shear properties below the superficial zone[23, 24]. This question was motivated by the observation that damage to immature cartilage (with our choice of injury) did not progress beyond the superficial zone[16]. Our data did exhibit a rise in the compressive properties with increasing tissue depth (Table I), consistent with several previous reports such as[22, 26, 28]. In particular, the ratios of the biomechanical properties (DZDs / SZDs) demonstrated a 2.62- (equilibrium modulus) and 7.32-fold rise (dynamic stiffness) between the two zones just below the superficial zone, which varied by up to one order of magnitude across a single sample. Thus, our data are consistent with the concept of an abrupt change in the properties at the interface between the superficial and the deeper zones [23, 24] suggestive of the concept of immature cartilage functioning as a bilayer composite.

Intrigued by the presence of zonally discrete biomechanical properties, we further investigated questions of depth-dependency in immature cartilage. On the used scale of measurement, the correlation of the depth position with both the compressive equilibrium properties and the dynamic stiffness of the immature cartilage samples did not reach significant levels when examining the SZDs or DZDs separately. However, the values of the properties of the two zones were significantly different from each other. Therefore, when analyzing the SZDs and DZDs as one statistically combined data set, both the equilibrium moduli and the dynamic stiffness correlated significantly with the depth position. These correlations suggest that immature articular functions as a bilayer composite material of zones whose interplay generates the known depth-dependent equilibrium properties of immature cartilage[28].

Next, we assessed whether the biomechanical properties correlated with sGAG because the compressive stiffness of articular cartilage is, among other factors, positively related to the fixed charge density of the sGAG content[28, 42]. The equilibrium moduli and the dynamic stiffness correlated with the sGAG content when SZDEs and DZDs were analyzed as statistically combined data but this correlation did not reach significance within SZDEs or DZDs that were analyzed separately. These data are consistent with the literature because it is known that both the sGAG content and the collagen content increase with depth and correlate with the compressive modulus [28].

Another study from our laboratory investigated the effects of injury to human knee cartilage from adult, non-degenerated post-mortem donors[35]. Counter-intuitively, increasing peak stress during injury was associated with less sGAG loss when the final (peak) strain and velocity were held constant[35]. In that study, the superficial zone was intentionally removed, and, effectively, samples comparable to our DZDs were analyzed. The study proposed that the cause of sGAG release was macro- or microstructural damage to the

cartilage matrix[35] rather than peak stress (which may well be the cause of the observed damage). In this context, we examined whether the stress-vs-time grades correlated with sGAG loss because the grading was based on discrete changes in the recorded stress, which, in turn, were caused by structural damage in the sense of stress yielding. Indeed, the correlation of stress-vs-time grades with sGAG loss reached significance suggesting that stress yielding was associated with sGAG loss from the damaged matrix. This finding is supported by another study[30]. However, we further investigated the counter-intuitive correlation of increasing peak stress with less sGAG loss that was observed in human adult samples comparable to our DZDs[35]. Our study confirmed that less sGAG was lost with more peak stress. However, this correlation was significant when both SZDEs and DZDs were analyzed as statistically combined data set; this correlation was not significant for DZDs or for SZDEs alone. The following conclusion can be drawn: immature cartilage and human cartilage sGAG loss are to some extend comparable but the relationship of sGAG loss with peak stress is zonally different between the two species.

One of the differences between SZDs and DZDs that may be important to the interpretation of our results was the difference in disk thickness between SZDs and DZDs. However, as seen in Fig 8, disk thickness had no significant effect on the stress-vs-time grades. The stress-vs-time grades classified the rise and time-course of stress during compressive injury and identified a potential stress loss under compression indicative of structural damage. Thus, our data demonstrated that the stress rise and specifically the loss of stress under injurious compression (caused by structural yielding) were independent of the thickness of the disk analyzed. In this context, the stress-vs-time grades were also independent of the occurring displacement rates, which in turn were caused by different disk thicknesses. These findings are important because previous studies often used the parameter “peak stress” to correlate biomechanical with biochemical data[34-36]. However, the present study demonstrated that both disk thickness and zonal origin have significant effects on peak stress.

In summary, based on the stress interpretation during compressive yielding, we present a novel biomechanical hypothesis and experiments to test the hypothesis that demonstrate the accurate prediction of structural damage during compressive injury. In a blinded experimental approach, we demonstrated that this method is sensitive enough to predict whether single cartilage matrix fractures or consecutive fractures occur. Based on the presence of zonally discrete biomechanical properties, we confirm the concept that immature articular functions as a bilayer composite material of zones whose overall depth-dependency is based on the interplay of zonally depth-independent biomechanical properties. Overall, our study illustrates that the biomechanical stress that occurs during compressive injury predetermines the biomechanical, biochemical, and structural consequences.

Acknowledgments

We gratefully thank MIT CBE members for their continuous support and friendship. We also thank Rita Kirsch for her excellent technical support. This work was funded in part by NIH grant R01-AR45779 (AG), DFG grants RO 2511/1-1 und 2-1 (BR), and the federal BMBF grant 01KQ0902B TP2 (BR).

Support: This work was funded in part by NIH grant R01-AR45779 (AG), DFG grants RO 2511/1-1 and 2-1 (BR), and the federal BMBF grant 01KQ0902B TP2 (BR).

References

1. Hjelle K, et al. Articular cartilage defects in 1,000 knee arthroscopies. Arthroscopy : the journal of arthroscopic & related surgery : official publication of the Arthroscopy Association of North America and the International Arthroscopy Association. 2002; 18(7):730–4. [PubMed: 12209430]
2. Lauterburg MT, Segantini P. Post-traumatic knee joint arthroscopy in children and adolescents. Schweizerische Zeitschrift fur Medizin und Traumatologie = Revue suisse pour medecine et traumatologie. 1994; (3):25–34. [PubMed: 7921792]
3. Smith GD, Knutsen G, Richardson JB. A clinical review of cartilage repair techniques. The Journal of bone and joint surgery. 2005; 87(4):445–9. British volume. [PubMed: 15795189]
4. Tallón-López J, Barón-Pérez Y, Flores-Ruiz MA. Arthroscopic Findings in Children's and Adolescents' Knees. Revista Española de Cirugía Ortopédica y Traumatología (English Edition). 2006; 51(5):237–244.
5. Stanitski CL, Harvell JC, Fu F. Observations on acute knee hemarthrosis in children and adolescents. Journal of pediatric orthopedics. 1993; 13(4):506–10. [PubMed: 8370785]
6. Sarpel Y, et al. Arthroscopy of the knee in pre-adolescent children. Archives of orthopaedic and trauma surgery. 2007; 127(4):229–34. [PubMed: 16830144]
7. Stanitski CL. Correlation of arthroscopic and clinical examinations with magnetic resonance imaging findings of injured knees in children and adolescents. The American journal of sports medicine. 1998; 26(1):2–6. [PubMed: 9474394]
8. Stanitski CL, Paletta GA Jr. Articular cartilage injury with acute patellar dislocation in adolescents. Arthroscopic and radiographic correlation. The American journal of sports medicine. 1998; 26(1): 52–5. [PubMed: 9474401]
9. Ure BM, et al. Arthroscopy of the knee in children and adolescents. European journal of pediatric surgery: official journal of Austrian Association of Pediatric Surgery (Zeitschrift fuer Kinderchirurgie). 1992; 2(2):102–5.
10. Oeppen RS, et al. Acute injury of the articular cartilage and subchondral bone: a common but unrecognized lesion in the immature knee. AJR Am J Roentgenol. 2004; 182(1):111–7. [PubMed: 14684522]
11. Mithofer K, et al. Functional outcome of knee articular cartilage repair in adolescent athletes. The American journal of sports medicine. 2005; 33(8):1147–53. [PubMed: 16000659]
12. Micheli LJ, et al. Articular cartilage defects of the distal femur in children and adolescents: treatment with autologous chondrocyte implantation. Journal of pediatric orthopedics. 2006; 26(4): 455–60. [PubMed: 16791061]
13. Macmull S, et al. Autologous Chondrocyte Implantation in the Adolescent Knee. The American journal of sports medicine. 2011
14. Bauer M, Jackson RW. Chondral lesions of the femoral condyles: a system of arthroscopic classification. Arthroscopy : the journal of arthroscopic & related surgery : official publication of the Arthroscopy Association of North America and the International Arthroscopy Association. 1988; 4(2):97–102. [PubMed: 3395426]
15. Ewers BJ, et al. The extent of matrix damage and chondrocyte death in mechanically traumatized articular cartilage explants depends on rate of loading. J Orthop Res. 2001; 19(5):779–84. [PubMed: 11562121]
16. Rolauffs B, et al. Vulnerability of the superficial zone of immature articular cartilage to compressive injury. Arthritis Rheum. 2010; 62(10):3016–27. [PubMed: 20556809]
17. Loening AM, et al. Injurious mechanical compression of bovine articular cartilage induces chondrocyte apoptosis. Arch Biochem Biophys. 2000; 381(2):205–12. [PubMed: 11032407]
18. Chen CT, et al. Time, stress, and location dependent chondrocyte death and collagen damage in cyclically loaded articular cartilage. J Orthop Res. 2003; 21(5):888–98. [PubMed: 12919878]
19. Repo RU, Finlay JB. Survival of articular cartilage after controlled impact. J Bone Joint Surg Am. 1977; 59(8):1068–76. [PubMed: 591538]
20. Hunziker, EB. Articular cartilage structure in humans and experimental animals, in Articular Cartilage and Osteoarthritis. Kuettner, KE.; Schleyerbach, R.; Peyron, JG.; Hascall, VC., editors. Raven Press; New York: 1992. p. 183-199.

21. Venn M, Maroudas A. Chemical composition and swelling of normal and osteoarthrotic femoral head cartilage. I. Chemical composition. Ann Rheum Dis. 1977; 36(2):121–9. [PubMed: 856064]
22. Schinagl RM, et al. Depth-dependent confined compression modulus of full-thickness bovine articular cartilage. J Orthop Res. 1997; 15(4):499–506. [PubMed: 9379258]
23. Buckley MR, et al. High-resolution spatial mapping of shear properties in cartilage. Journal of biomechanics. 2010; 43(4):796–800. [PubMed: 19896130]
24. Buckley MR, et al. Mapping the depth dependence of shear properties in articular cartilage. J Biomech. 2008; 41(11):2430–7. [PubMed: 18619596]
25. Chen AC, et al. Depth- and strain-dependent mechanical and electromechanical properties of full-thickness bovine articular cartilage in confined compression. J Biomech. 2001; 34(1):1–12. [PubMed: 11425068]
26. Chen SS, et al. Depth-dependent compressive properties of normal aged human femoral head articular cartilage: relationship to fixed charge density. Osteoarthritis Cartilage. 2001; 9(6):561–9. [PubMed: 11520170]
27. Grodzinsky AJ. Electromechanical and physicochemical properties of connective tissue. Crit Rev Biomed Eng. 1983; 9(2):133–99. [PubMed: 6342940]
28. Klein TJ, et al. Depth-dependent biomechanical and biochemical properties of fetal, newborn, and tissue-engineered articular cartilage. J Biomech. 2007; 40(1):182–90. [PubMed: 16387310]
29. Sui Y, et al. Mechanical injury potentiates proteoglycan catabolism induced by interleukin-6 with soluble interleukin-6 receptor and tumor necrosis factor alpha in immature bovine and adult human articular cartilage. Arthritis Rheum. 2009; 60(10):2985–96. [PubMed: 19790045]
30. DiMicco MA, et al. Mechanisms and kinetics of glycosaminoglycan release following in vitro cartilage injury. Arthritis Rheum. 2004; 50(3):840–8. [PubMed: 15022326]
31. Kurz B, et al. Pathomechanisms of cartilage destruction by mechanical injury. Ann Anat. 2005; 187(5-6):473–85. [PubMed: 16320827]
32. Lee JH, et al. Mechanical injury of cartilage explants causes specific time-dependent changes in chondrocyte gene expression. Arthritis Rheum. 2005; 52(8):2386–95. [PubMed: 16052587]
33. Morel V, Quinn TM. Cartilage injury by ramp compression near the gel diffusion rate. J Orthop Res. 2004; 22(1):145–51. [PubMed: 14656673]
34. Quinn TM, et al. Matrix and cell injury due to sub-impact loading of adult bovine articular cartilage explants: effects of strain rate and peak stress. J Orthop Res. 2001; 19(2):242–9. [PubMed: 11347697]
35. Patwari P, et al. Analysis of the relationship between peak stress and proteoglycan loss following injurious compression of human post-mortem knee and ankle cartilage. Biomech Model Mechanobiol. 2007; 6(1-2):83–9. [PubMed: 16715319]
36. Kurz B, et al. Biosynthetic response and mechanical properties of articular cartilage after injurious compression. J Orthop Res. 2001; 19(6):1140–6. [PubMed: 11781016]
37. Flachsmann R, Broom ND, Hardy AE. Deformation and rupture of the articular surface under dynamic and static compression. J Orthop Res. 2001; 19(6):1131–9. [PubMed: 11781015]
38. Asanbaeva A, et al. Regulation of immature cartilage growth by IGF-I, TGF-beta1, BMP-7, and PDGF-AB: role of metabolic balance between fixed charge and collagen network. Biomech Model Mechanobiol. 2008; 7(4):263–76. [PubMed: 17762943]
39. Mow VC, Guo XE. Mechano-electrochemical properties of articular cartilage: their inhomogeneities and anisotropies. Annu Rev Biomed Eng. 2002; 4:175–209. [PubMed: 12117756]
40. Frank EH, et al. A versatile shear and compression apparatus for mechanical stimulation of tissue culture explants. J Biomech. 2000; 33(11):1523–7. [PubMed: 10940414]
41. Farndale RW, Buttle DJ, Barrett AJ. Improved quantitation and discrimination of sulphated glycosaminoglycans by use of dimethylmethylene blue. Biochim Biophys Acta. 1986; 883(2):173–7. [PubMed: 3091074]
42. Armstrong CG, Mow VC. Variations in the intrinsic mechanical properties of human articular cartilage with age, degeneration, and water content. J Bone Joint Surg Am. 1982; 64(1):88–94. [PubMed: 7054208]

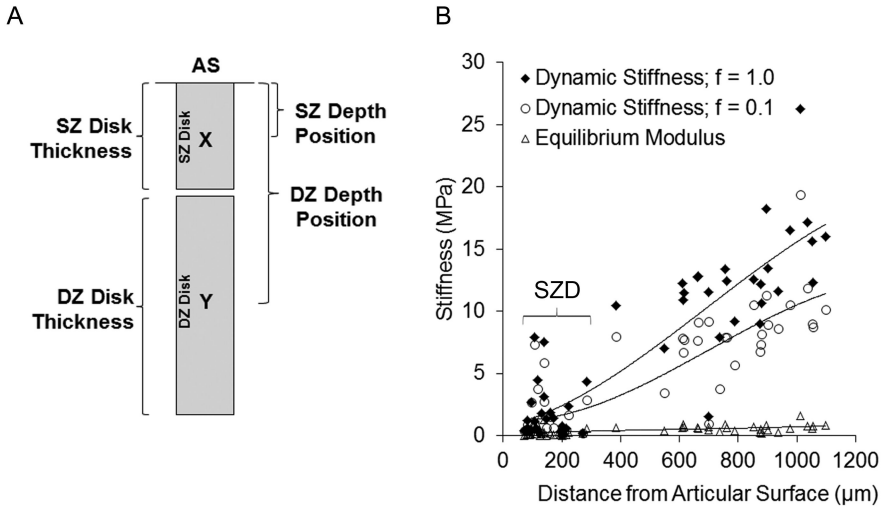

Figure 1. Calculation of the depth-position & biomechanical characterization of cartilage disks before injury

(A) The depth position (distance from the articular surface) was calculated for each disk (superficial zone disk: SZD (n=32); deeper zones disk: DZD (n=32)) to assess the distance of each disk center (x and y) from the articular surface (AS). x and y were calculated as follows: x = 1/2*SZ disk thickness; y = SZ disk thickness + 1/2*DZ disk thickness. (B) Dynamic stiffness and equilibrium modulus vs. depth position (distance from the articular surface to the center of a SZD (x) or DZD (y)) as scatter plot with regression lines. For both frequencies 0.1 and 1Hz, the non-linear regression reached significant levels when both SZDs and DZDs were statistically analyzed as one data set (as shown) and when the DZDs but not the SZDs were analyzed separately. For the equilibrium modulus vs. depth position, linear regression reached significant levels when both SZDs and DZDs were statistically analyzed as one data set (as shown).

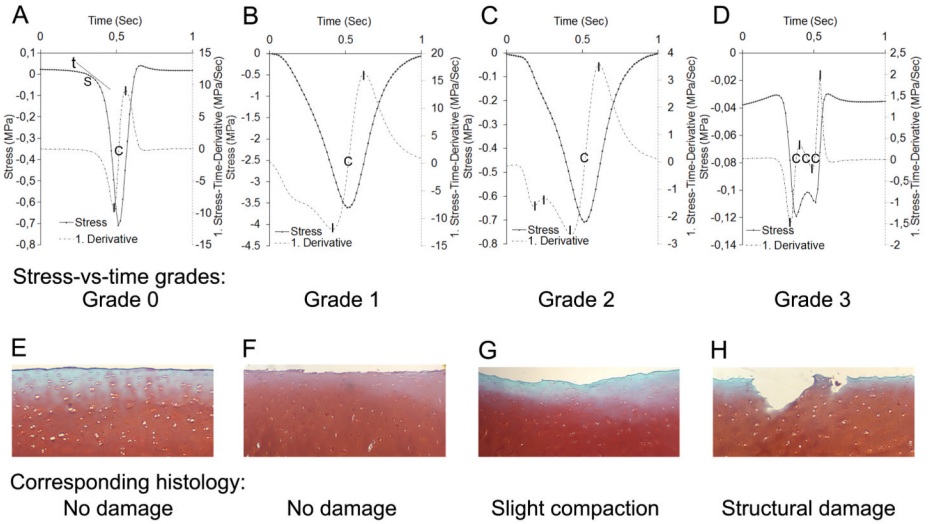

Figure 2. Typical Stress-vs-time signals, their time-derivatives (to identify the maximum stress rise), and the corresponding histology

(A) Representative stress-vs-time signal of a Grade 0 SZD (negative stress indicates compression). Its derivative was characterized by 1 critical (C) and 2 inflection (I) points. S: sample stress-vs-time point, for which the derivative was determined from the slope of the tangent line (t). The corresponding histology of an injured SZD that remained undamaged is shown in (E). (B) Representative stress-vs-time signal of a Grade 1 SZD. The derivative revealed a lower magnitude stress rise over time, though still characterized by 1 critical and 2 inflection points. The corresponding histology of an injured SZD that remained undamaged is shown in (F). (C) SZD Grade 2 stress-vs-time signal whose derivative showed a local decrease with time during the compression phase and was characterized by 1 critical point and 4 inflection points. The corresponding histology of an injured SZDE (superficial zone damaged explant) that suffered compaction is shown in (G). (D) Grade 3 stress-vs-time signal with the presence of a double tip instead of a single tip at the transition from compression to relaxation indicating a pronounced stress loss during the final stage of injurious compression. The derivative was characterized by 3 critical points and 4 inflection points. The corresponding histology of an injured SZDE that suffered extensive structural damage is shown in (G).

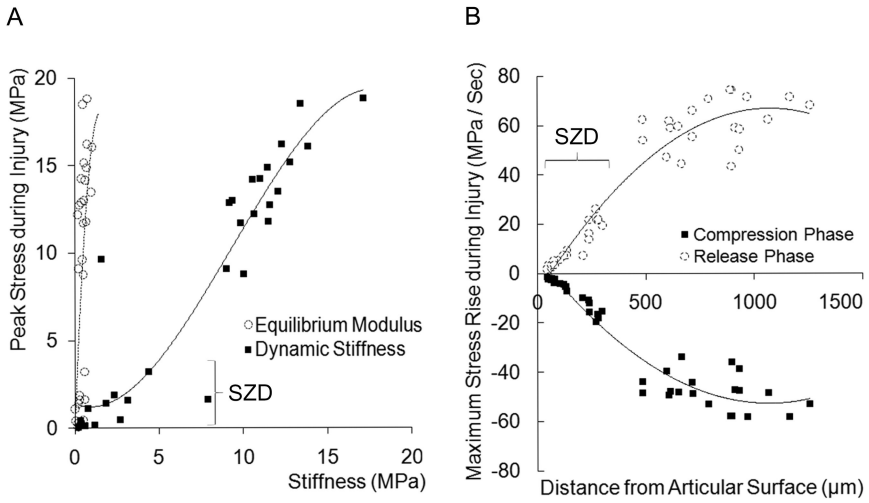

Figure 3. Peak stress and maximum stress rise of the occurring stress during injury

(A) Scatter plot and non-linear regression of the peak stress (measured during injury) vs. equilibrium modulus (white markers) and dynamic stiffness at f=1Hz (black markers); (B) Scatter plot and non-linear regression of the maximum stress rise vs. depth position (distance from the articular surface; positive values: compression, negative values: relaxation; SZD: superficial zone disk).

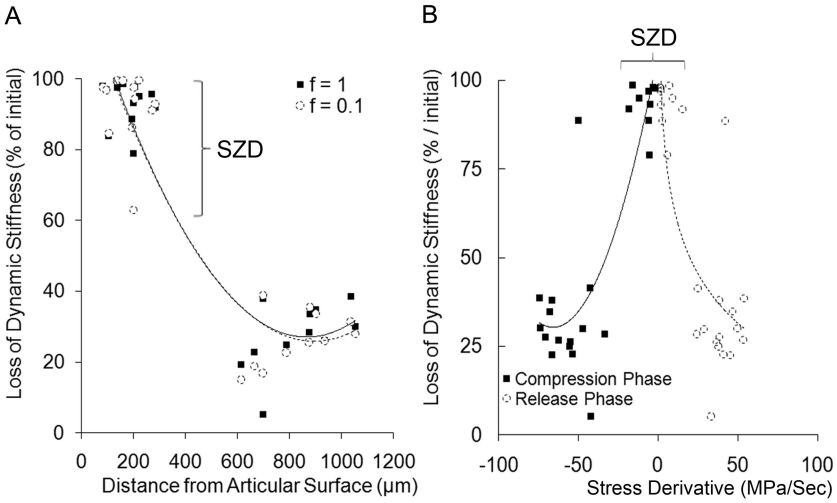

Figure 4. Biomechanical impairment after injury

(A) Scatter plot and non-linear regression of the loss of dynamic stiffness vs. depth position and (B) the loss of dynamic stiffness vs. the stress derivative during injury ; SZDE: superficial zone disk.

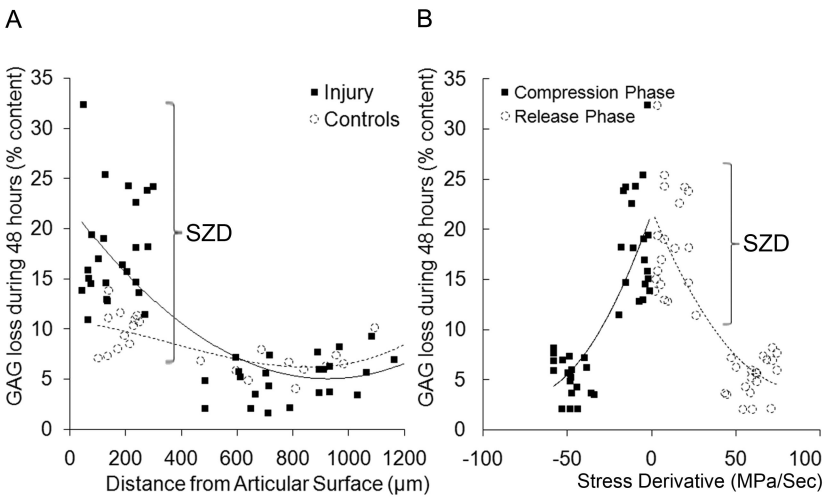

Figure 5. Biochemical impairment after injury

(A) Scatter plot and non-linear regression of the loss of sGAG vs. depth position and (B) the loss of sGAG vs. stress derivative during injury; SZDE: superficial zone disk.

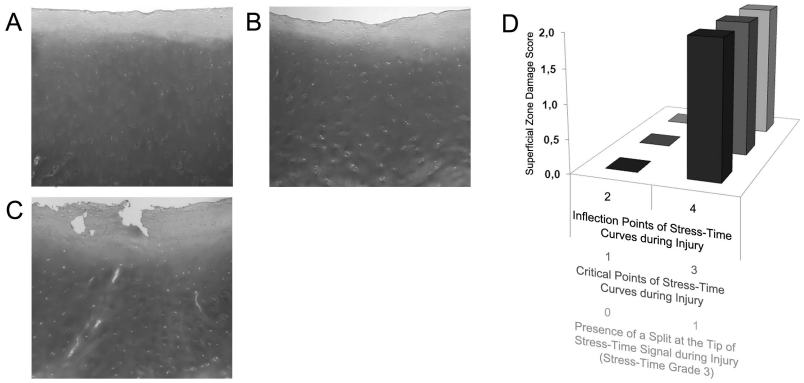

Figure 6. Histological analysis and correlation with stress-vs-time signals

Representative images of (A) an uninjured control disk without damage, (B) an injured disk with slight compaction but without structural damage, and (C) an injured disk with slight compaction and structural damage such as matrix disruption. (D) The damage score and stress-vs-time signal characterization of injured and structurally damaged disks. In injured disks, the presence of histological damage correlated with the presence of 4 inflection points, 3 critical points, and the presence of a split at the signal tip (see Fig. 2). Damage score grade 0=normal appearing cartilage with proper staining in each zone except the intact superficial zone with the surface showing no signs of damage; grade 1=minimal surface damage with isolated disruptions; grade 2=moderate surface damage with widespread disruption; grade 3=minimal permanent compression; grade 4=permanent compression to approximately ≥ 30% of the original disk thickness.

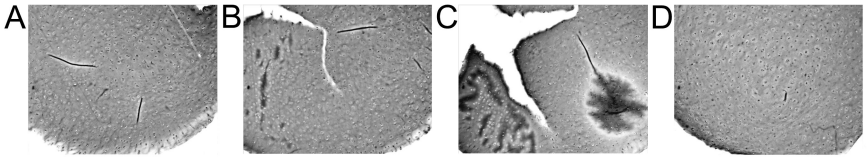

Figure 7. Histological analysis for damage prediction of injured disks

Representative images of serial sections of (A) an uninjured control disk without damage, (B) an injured disk with a single horizontal matrix disruption, whose corresponding stress-vs-time signal contained a double tip (stress-vs-time grade 3; see Fig. 3D), (C) an injured disk with a horizontal matrix disruption pervading the disk in a y-shape whose corresponding stress-vs-time signal contained a triple tip (stress-vs-time grade 3), (D) an injured disk whose stress-vs-time signal was graded as 1 (Fig. 2B).

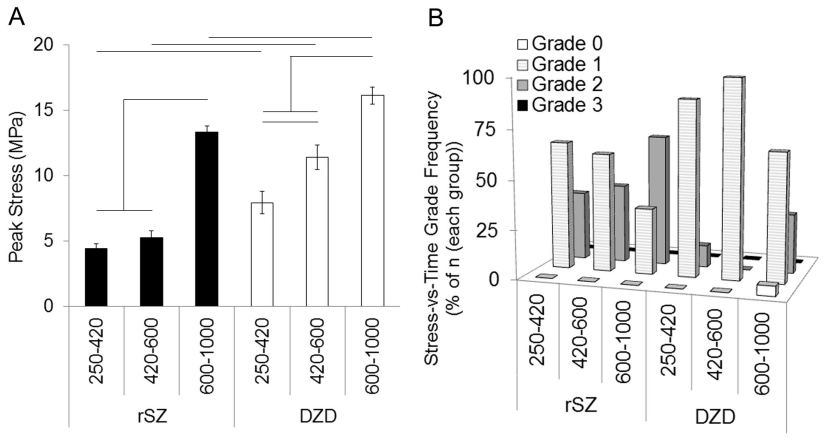

Figure 8. Effects of disk thickness and zonal origin on peak stress and stress-vs-time grades

Three additional sets of disks with retained superficial zone (rSZ; n=28) were prepared with thicknesses ranging from 250-420μm, 420-600μm, and 600-1000μm and compared to 3 sets of DZDs with comparable thickness ranges. The differences in the peak stress (A) between each set of rSZ and the corresponding DZD set indicated a zonal effect on peak stress. When comparing the 3 rSZ sets with each other, the peak stress of the set with 600-1000μm thickness was significantly higher than the other 2 sets having lower thickness. The same was true for the DZD sets which, together, suggest an effect of thickness on peak stress. (B) There were no significant differences in the stress-vs-time grades between each set of rSZ and the corresponding DZD set, suggesting that there was no zonal effect on the stress-vs-time grades. When comparing the 3 rSZ sets with each other, the stress-vs-time grades were not significantly different. The same was true for the DZD sets which, together, suggest that there was no effect of thickness on the stress-vs-time grades.

TABLE I

REGRESSION AND CORRELATION

				Non-linear Regression Level of Significance			Pearson Product Moment Correlation Level of Significance		
Timeline	**Vertical Axis**	**Horizontal Axis**	Frequency	**S&D**	**s**	**D**	**S&D**	**S**	**D**
Pre-Injury	GAG content	Depth Position (μm)	X	< 0.001	< 0.05	n.s.	< 0.0001	< 0.01	< 0.05
	Equilibrium Modulus (MPa)	Depth Position (μm)	X	< 0.001	n.s.	n.s.	< 0.0001	n s.	n.s.
	Equilibrium Modulus (MPa)	GAG content	X	<0.01	n.s.	n.s.	< 0 05	n.s.	n.s.
	Dynamic Stiffness (MPa)	Depth Position (μm)	f= 1.0	< 0.001	n.s.	<0.05	< 0.0001	n.s.	< 0.01
		Depth Position (μm)	f = 0.8	< 0.001	n.s.	<0.05	< 0.0001	n.s.	<0.01
		Depth Position (μm)	f = 0.5	< 0.001	n.s.	< 0.05	< 0.0001	n.s.	< 0.01
		Depth Position (μm)	f = 0.3	< 0.001	n.s.	<0.05	< 0.0001	n s.	< 0.01
		Depth Position (μm)	f = 0.2	< 0 001	n.s.	<0.05	< 0.0001	n.s.	< 0.01
		Depth Position (μm)	f = 0.1	< 0.001	n.s.	<0.05	< 0.0001	n.s.	< 0.01
	Dynamic Stiffness (MPa)	GAG content	f= 1.0	< 0.0001	n.s.	n.s.	< 0.0001	n.s.	n.s.
	Equilibrium Modulus (MPa)	Initial Dynamic Stiffness (MPa)	f= 1.0	< 0.001	< 0.001	<0.01	< 0.0001	< 0.0001	< 0.0001
			f = 0.1	< 0.001	< 0.001	<0.01	< 0.0001	< 0.0001	< 0.0001
Injury	Peak Stress (MPa)	Depth Position (μm)	X	< 0.001	n.s.	n.s.	< 0.0001	n.s.	n.s.
	Peak Stress (MPa)	Initial Equilibrium Modulus (MPa)	X	<0.01	n.s.	n.s.	< 0.001	n.s.	n.s.
	Peak Stress (MPa)	Initial Dynamic Stiffness (MPa)	f= 1.0	< 0.001	n.s.	n.s.	< 0.0001	<0.05	< 0.0001
			f = 0.1	< 0.001	n.s.	n.s.	< 0.0001	n.s.	< 0.01
	Maximum Stress Rise during Injury (Compression)	Depth Position (μm)	X	< 0.0001	< 0.0001	n.s.	< 0.0001	< 0.0001	n.s.
	Maximum Stress Rise during Injury (Release)	Depth Position (μm)	X	< 0 0001	< 0.0001	n.s.	< 0.0001	< 0.0001	n.s.
	Loss of Dynamic Stiffness (%)	Depth Position (μm)	f= 1.0	< 0.001	n.s.	n.s.	< 0.0001	n.s.	n.s.
			f = 0.1	< 0.001	n.s.	n.s.	< 0.0001	n.s.	n.s.
	Loss of Dynamic Stiffness (%)	Peak Stress (MPa)	f = 1.0	< 0.001	n.s.	n.s.	< 0.0001	n.s.	n.s.
			f = 0.1	< 0.001	n.s.	n.s.	< 0.0002	n s.	n.s.
	Loss of Dynamic Stiffness (%)	Dissipated Energy during Injury	f = 1.0	< 0.0001	n.s.	n.s.	< 0.0001	n.s.	n.s.
	Loss of Dynamic Stiffness (%)	Maximum Stress Rise during Injury (Compression)	f = 1.0	< 0.0001	n.s.	n.s.	< 0.0001	n.s.	n.s.
	Loss of Dynamic Stiffness (%)	Maximum Stress Rise during Injury (Release)	f= 1.0	< 0.0001	n.s.	n.s.	< 0.0001	n.s.	n.s.
	Loss of Dynamic Stiffness (%)	Stress-Time Grading	X	X	X	X	< 0.05	< 0.05	n.s.

				Non-linear Regression Level of Significance			Pearson Product Moment Correlation Level of Significance		
	Loss of Dynamic Stiffness (%)	Displacement Rate	X	< 0.0001	n.s.	<0.05	< 0.0001	n s.	< 0.01
	Strain Rate	Stress-Time Grading	X	X	X	X	n.s.	<0.05	< 0.001
	Presence of histological damage	Stress-Time Grading	X	X	X	X	X	< 0.001	X
	Dissipated Energy during Injury	Depth Position (μm)	X	< 0.0001	n.s.	n.s.	< 0.0001	n.s.	n.s.
	Dissipated Energy during Injury	Maximum Stress Rise during Injury (Compression)	X	< 0.001	< 0.0001	<0.01	< 0.0001	< 0.0001	< 0.01
	Dissipated Energy during Injury	Maximum Stress Rise during Injury (Release)	X	< 0.001	< 0.05	< 0.05	< 0.0001	< 0.01	< 0.05
Post-Injury	GAG loss (% / Content)	Depth Position (μm)	X	< 0.001	n.s.	n.s.	< 0.0001	n s.	< 0.05
	GAG loss (% / Content)	Peak Stress (MPa)	X	< 0.0001	n.s.	n.s.	< 0.0001	n.s.	n.s.
	GAG loss (% / Content)	Dissipated Energy during Injury	X	< 0.0001	n.s.	n.s.	< 0.0001	n.s.	n.s.
	GAG loss (% / Content)	Maximum Stress Rise during Injury (Compression)	X	< 0.0001	n.s.	n.s.	< 0.0001	n.s.	n.s.
	GAG loss (% / Content)	Maximum Stress Rise during Injury (Release)	X	< 0.0001	n.s.	n.s.	< 0.0001	n.s.	n.s.
	GAG loss (% / Content)	Displacement Rate	X	< 0.0001	n.s.	n.s.	< 0.0001	n s.	n.s.
	GAG loss (% / Content)	Stress-Time Grading	X	X	X	X	< 0.05	n.s.	n.s.
Controls	GAG loss (% / Content)	Depth Position (μm)	X	<0.01	n.s.	n.s.	< 0.01	n.s.	n.s.

S&D: the superficial and deeper zones disks were analyzed together; S: the superficial zone disks were analyzed seperately; D: the deeper zones disks were analyzed seperately.

X: not applicable.

* best fit was linear

** linear correlation (non-linear correlation was not significant)

§ correlation based on ranks

no marker: best fit was non-linear